# $^1$H NMR Solution Structure of an Active Monomeric Interleukin-8[†,||]

Krishnakumar Rajarathnam,[‡] Ian Clark-Lewis,[§] and Brian D. Sykes*[,‡]

*Protein Engineering Network of Centres of Excellence and Department of Biochemistry, University of Alberta, Edmonton, Alberta, Canada T6G 2S2, and Protein Engineering Network of Centres of Excellence and Department of Biochemistry, University of British Columbia, Vancouver, British Columbia, Canada V6T 1Z3*

*Received May 31, 1995*[⊗]

ABSTRACT: The solution structure of a monomeric form of interleukin-8 (IL-8) has been solved using $^1$H NMR spectroscopy. The chemically synthesized nonnatural analog {IL-8 (4−72) L25 NH → $NCH_3$} has the same activity as that of native IL-8. Thirty structures were generated using the hybrid distance geometry and simulated annealing protocol using the program X-PLOR. The structure is well-defined except for N-terminal residues 4−6 and C-terminal residues 67−72. The rms distribution about the average structure for residues 7−66 is 0.38 Å for the backbone atoms and 0.87 Å for all heavy atoms. The structure consists of a series of turns and loops followed by a triple-stranded $\beta$ sheet and a C-terminal $\alpha$ helix. The structure of the monomer is largely similar to the native dimeric IL-8 structures previously determined by both NMR and X-ray methods. The major difference is that, in the monomeric analog, the C-terminal residues 67−72 are disordered whereas they are helical in the two dimeric structures. The best fit superposition of the backbone atoms of residues 7−66 of the monomer structure on the dimeric IL-8 structures showed rms differences of 1.5 and 1.2 Å respectively. The turn (residues 31−35), which is disulfide linked to the N-terminal region, adopts a conformation in the monomer similar to that seen in the dimeric X-ray structure (rms difference 1.4 Å) and different from that seen in the dimeric NMR structure (rms difference 2.7 Å). The structural data indicate that the constraints imposed by dimerization are not critical either for the tertiary fold or for functional activation of IL-8.

Interleukin-8 (IL-8)[1] is a chemotactic cytokine (chemokine) that promotes the accumulation and activation of neutrophils and has been implicated in a number of acute and chronic inflammatory diseases (Baggiolini et al., 1994; Miller & Krangel, 1992). It is the best studied of a family of human neutrophil activating proteins that are characterized by the sequence E-L-R-C-X-C near the N-terminus. The structure and function of IL-8 have been extensively characterized, and IL-8 serves as a prototype for this family of proteins (Clark-Lewis et al., 1991, 1995; Rajarathnam et al., 1994a). The structure of IL-8 has been solved by both NMR and X-ray methods, and both techniques showed IL-8 to be a noncovalent homodimer (Clore et al., 1990; Baldwin et al., 1991).

To address the importance of the dimeric state for receptor binding and function, we had chemically synthesized a monomeric IL-8 analog (L25NMe) by modifying the amide of Leu-25 into *N*-methyl (Figure 1). This analog displayed functional characteristics similar to those of the native protein

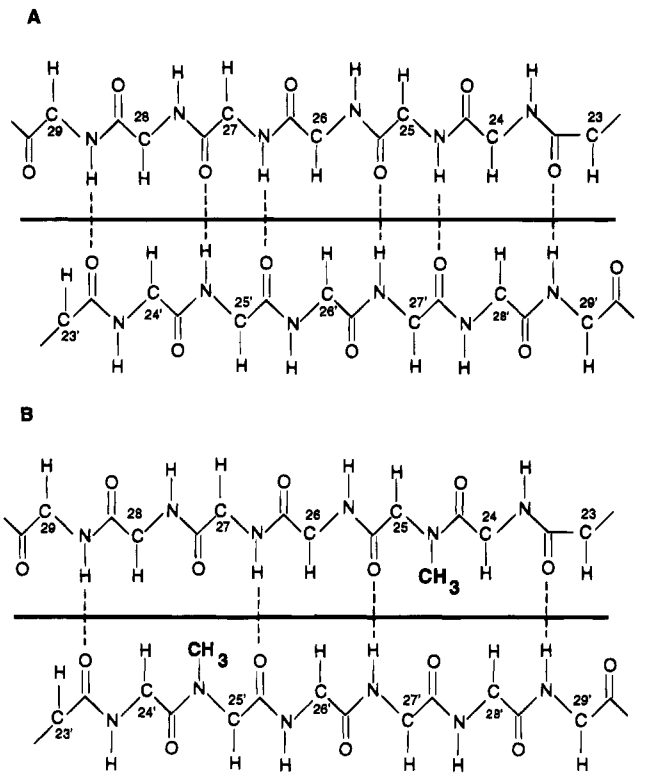


FIGURE 1: Schematic presentation of (A) the dimer interface in the native interleukin-8 showing the hydrogen bonding by dotted lines and (B) the L25NMe analog in which the NH has been chemically modified to $NCH_3$ (NH → $NCH_3$).

[†] This work is supported by grants from the Protein Engineering Network of Centres of Excellence.

[||] Coordinates have been deposited with the Brookhaven Protein Data Bank under Accession Codes 1IKL for the minimized average structure and 1IKM for the ensemble of 30 SA structures.

* To whom correspondence should be addressed.

[‡] University of Alberta.

[§] University of British Columbia.

[⊗] Abstract published in *Advance ACS Abstracts,* September 15, 1995.

[1] Abbreviations: IL-8, interleukin-8; NAP-2, neutrophil-activating peptide-2; MGSA, melanoma growth stimulatory activity; PF-4, platelet factor-4; IP-10, $\gamma$-interferon-induced protein; MIP-1$\beta$, macrophage inflammatory protein-1$\beta$; RANTES, regulated upon activation, normal T-cell expressed, and presumably secreted; NMR, nuclear magnetic resonance; DQF-COSY, double-quantum-filtered correlated spectroscopy; NOE, nuclear Overhauser enhancement; NOESY, nuclear Overhauser enhancement spectroscopy; PE-COSY, primitive exclusive correlation spectroscopy; ROESY, rotating frame nuclear Overhauser spectroscopy; TOCSY, total correlated spectroscopy; rms, root mean square; SA, simulated annealing; ppm, parts per million; DSS, 2,2-dimethyl-2-silapentane-5-sulfonic acid.

0006-2960/95/0434-12983$09.00/0 

and was shown to be a monomer by sedimentation equilibrium and NMR studies (Rajarathnam et al., 1994b). Two independent studies using a variety of techniques including sedimentation equilibrium, fluorescence anisotropy, and microcalorimetry methods obtained monomer−dimer $K_d$ values for native IL-8 of ~20 $\mu$M (Burrows et al., 1994; Paolini et al., 1994). These $K_d$ values suggest that at physiological concentrations (~0.1−10 nM), the dominant species is the monomer. Thus the dimeric structure of native IL-8 does not represent the form that binds to the receptor. Because the monomer exists at such dilute concentrations, the tertiary structure of the native monomer cannot be obtained with any of the current physical methods available. However, the L25NMe analog is monomeric at all concentrations tested. We have solved the structure of the monomeric IL-8 L25NMe analog by two-dimensional $^1$H NMR spectroscopy and report herein the structural features of the monomer and discuss the implications of its structure for receptor binding and functional activation.

## MATERIALS AND METHODS

*Sample Preparation.* The L25NMe (4−72) monomeric analog[2] was chemically synthesized, purified, and characterized as discussed in detail previously (Rajarathnam et al., 1994b; Clark-Lewis et al., 1991). The protein concentrations for the NMR samples were ~2 mM in 20 mM sodium acetate buffer, pH ~5.2 (uncorrected for isotope effect).

*NMR Methods.* All $^1$H NMR experiments were performed on a Varian Unity 600 spectrometer. Resonances were assigned from DQF-COSY (Rance et al., 1983), TOCSY (Davis & Bax, 1985), ROESY (Bothner-By et al., 1984), and NOESY experiments (Jeener et al., 1979). The data were collected over a temperature range of 20 to 40 °C, which greatly aided in resolving almost all of the amide resonances. The NOESY and TOCSY were collected over 2K points, and DQF-COSY was collected over 4K points along $t_2$ and 256−500 increments along $t_1$. The quadrature detection along the $t_1$ dimension was achieved as described by States et al. (1982). The solvent was suppressed using presaturation, and for NOESY and DQF-COSY experiments, the loss of intensity of the cross peaks near the $H_2O$ signal was minimized using the SCUBA sequence (Brown et al., 1988). NOESY spectra were collected at 50, 100, and 150 ms mixing times for structure determinations, and the TOCSY spectra were acquired with a mixing time of 55 ms. A PE-COSY with a 36° mixing pulse was also collected in $^2H_2O$ (Mueller, 1987). The NOESY and TOCSY spectra were processed using a Gaussian function with resolution enhancement or shifted sine-bell function, and DQF-COSY spectra were processed using a sine-bell function. In all cases, the spectra were zero-filled to 2K × 2K points except for the DQF-COSY spectra which were zero-filled to 8K × 1K. All spectra are referenced to the internal DSS at 0.00 ppm.

*NOE-Derived Distance Restraints.* NOE cross-peak intensities were classified as strong, medium, or weak, corresponding to upper distance restraints of 2.7, 3.5, and 5 Å, respectively, on the basis of a 150 ms NOESY spectrum.

[2] The IL-8 (4−72) analog missing the first three residues had a slightly higher activity than the native IL-8 (1−72). Hence the L25NMe analog was synthesized in the 4−72 form.

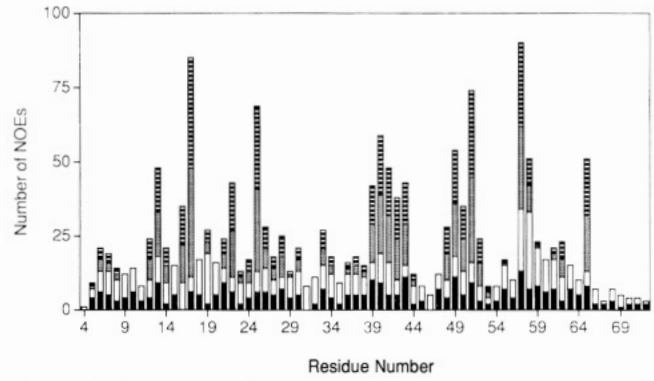


FIGURE 2: Summary of the number and the nature of the NOE constraints per residue versus the amino acid number. The nature of NOEs and the corrersponding symbols are as follows: intraresidue (black), sequential (open), medium-range (cross-hatched), and long-range NOEs (vertically hatched).

Upper limits for nonstereospecifically assigned methyl and methylene protons were corrected appropriately (Wüthrich et al., 1983). In addition, 0.5 Å was added to the upper boundaries to correct for higher intensities for distances involving methyl protons (Clore et al., 1987).

*Torsion Restraints and Stereospecific Assignments.* Backbone $\phi$ angles were calculated from the coupling constants measured from the DQF-COSY spectrum using the method of Kim and Prestagard (1989). Stereospecific assignments and $\chi_1$ restraints were obtained from the analysis of the $^3J_{\alpha\beta}$ coupling constants and the relative intensities of the NOEs from the NH and the $C^\alpha H$ to the $C^\beta H$ protons on the basis of the NOESY spectrum at 50 ms and the ROESY spectrum at 30 ms. In the latter stage of the refinement, the methyl groups of Val-27, -41, -58, and -61 and Leu-43, -49, and -51 could be stereospecifically assigned on the basis of intraresidue NOEs (Basus, 1989; Powers et al., 1993).

*Hydrogen Bond Restraints.* The potential candidates for hydrogen bonding were initially identified on the basis of observing slow exchanging amide protons in a COSY spectrum recorded within 12 h of dissolving the protein in $^2H_2O$. For each hydrogen bond, two distance restraints were used ($r_{NH-O}$, 1.8−2.3 Å, and $r_{N-O}$, 2.4−3.3 Å). The hydrogen-bonding restraints were used only after an initial set of structures had been calculated. Only the amide protons which satisfied distance and angular restraints with hydrogen bond acceptors were used in the structure calculations (Wagner et al., 1987).

*Structure Calculations.* Structures were calculated by the hybrid distance geometry−dynamical simulated annealing method (Nilges et al., 1988) using the program X-PLOR (Brünger, 1992). A total of 903 NOE distance restraints (331 intraresidue, 249 sequential, 118 medium-range, and 205 long-range NOEs) were used. The distribution of the NOEs along the amino acid sequence is shown in Figure 2. In addition, 61 dihedral restraints (40 $\phi$ and 21 $\chi_1$) and 24 hydrogen-bonding restraints (from 12 hydrogen bonds) were used in the final structure calculations. The initial structures were generated with NOE restraints alone, and in subsequent structure calculations, the dihedral and hydrogen bond restraints were included. The simulated annealing calculations were carried out using the standard force-field parameter set (parallhdg.pro) and topology file (topallhdg.pro) in X-PLOR version 3.1.

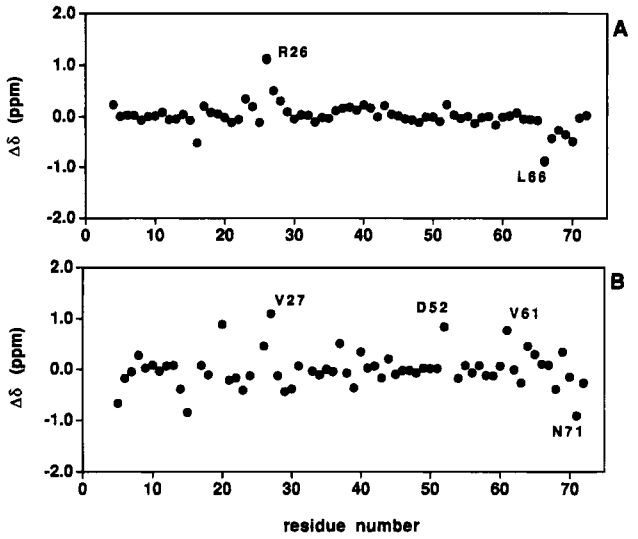


FIGURE 3: Plots of the $^1$H NMR chemical shift differences of the (A) C$^\alpha$H and (B) NH resonances between the native dimeric IL-8 and the monomeric L25NMe analog versus the residue number. Some of the C$^\alpha$H and amide protons which show large differences between the two proteins are labeled. A positve chemical shift difference implies a larger chemical shift in the native dimer.

## RESULTS AND DISCUSSION

*Chemical Shift Analysis.* A complete list of the $^1$H NMR chemical shifts of the monomeric IL-8 (L25NMe) analog is given in the supporting information. The assignments were accomplished using standard two-dimensional NMR techniques (Wüthrich, 1986). Scalar connectivities were identified from the TOCSY and DQF-COSY spectra, and through-space connectivities were identified from the NOESY spectra. The chemical shifts of the spin systems were fairly well dispersed, and in case of overlap, the chemical shifts could be resolved by collecting the TOCSY and the NOESY data at different temperatures (20−40 °C). A number of protons with large upfield and downfield chemical shifts are seen in both the dimer and the monomer including the amide protons of Gln-8, Lys-20, Lys-15, Phe-17, and Val-58 and the C$^\alpha$H of Pro-16, Cys-50, and Val-58. The observation that these shifts are essentially the same in the monomeric L25NMe analog suggests similar secondary and tertiary structural environments for these residues. Figure 3 shows the difference between the monomeric and dimeric proteins in the chemical shifts of the C$^\alpha$H and the amide protons. C$^\alpha$H shifts are sensitive indicators of secondary and tertiary structure (Wishart et al., 1991). The largest perturbation in chemical shifts was observed for residues at the dimer interface: residues 24−29 constituting the first $\beta$ strand and residues 65−69 at the C-terminal α helix (Figure 3A). No simple correlation exists between amide proton chemical shifts and structure. It has been suggested that, in addition to secondary and tertiary structures, they are also sensitive to factors such as hydrogen-bonding, nearest neighbor, or sequence effects and solvent exposure which may be related to the dynamics of the protein (Wishart et al., 1991; Pardi et al., 1983). Indeed, it is seen that, in addition to significant changes in chemical shifts for protons at the dimer interface (Figure 3B), large chemical shift differences are also observed for other protons, suggesting significant changes in dynamic properties between the proteins.

Table 1: Structural Statistics and Atomic rms Differences of the Interleukin-8 Monomer[a]

| (A) Structural Statistics | ⟨SA⟩ | (SA)r |
|---|---|---|
| rms deviation from exptl distance restraints (Å) (913) | 0.044 ± 0.001 | 0.044 |
| rms deviation from exptl dihedral restraints (deg) (61) | 0.31 ± 0.11 | 0.30 |
| deviations from ideal geometry | | |
| bonds (Å) | 0.0046 ± 0.0001 | 0.0047 |
| angles (deg) | 0.71 ± 0.01 | 0.71 |
| improper (deg) | 0.51 ± 0.01 | 0.52 |

| (B) Atomic rms Differences (Residues 7−66) (Å) | backbone atoms | heavy atoms |
|---|---|---|
| ⟨SA⟩ vs SA | 0.38 ± 0.08 | 0.87 ± 0.06 |
| ⟨SA⟩ vs (SA)$_r$ | 0.51 ± 0.10 | 1.07 ± 0.08 |
| SA vs (SA)$_r$ | 0.35 | 0.61 |

[a] The notations are as follows: ⟨SA⟩ are the 30 final simulated annealing structures; SA is the mean structure obtained by averaging the coordinates of the 30 individual structures (residues 7−66); (SA)$_r$ is the restrained minimized average structure obtained by restrained minimization of SA.

*Structural Statistics of the Monomeric IL-8 (L25NMe).* The statistics of the 30 final simulated annealing (SA) structures are shown in Table 1, and the superimposition of the individual structures on the average structure is shown in Figure 4. Most of the protein is well-defined except for residues 4−6 and 67−72. The quality of the generated structures was tested using the programs PROCHECK (Laskowski et al., 1993) and VADAR (Wishart et al., 1994) for various criteria such as the stereochemistry, hydrogen bonds, the region of occupancy in the Ramachandran plot, van der Waals contacts, buried charged residues, number of buried residues, and packing defects. All 30 structures met the criteria that is expected of a high-resolution structure.

All 30 SA structures and the energy-minimized average structure displayed good covalent geometry (Table 1) and minimal NMR constraint violations. None of the 30 SA structures had NOE violations greater than 0.5 Å and dihedral angle violations greater than 5°. There were a total of five nonsystematic NOE violations greater than 0.3 Å and two dihedral angle violations greater than 3°. The rms distribution for residues 7−66 between all 30 structures and the average structure is 0.38 Å for the backbone atoms and 0.87 Å for the heavy atoms (Figure 5 A,B). The precision of the torsion angles is assessed in terms of the order parameter $S$ (Hyberts et al., 1992; Pallaghy et al., 1993). The angular order parameter is a statistical parameter such that when the value of an angle is identical for all members of a family of structures, the value of $S = 1$, and for a completely undefined angle, the value of $S = 0$. Typically, $S$ values of 1.00, 0.99, 0.98, and 0.90 correspond to angular standard deviations of 0°, 8°, 18°, and 26° respectively (Hyberts et al., 1992; Pallaghy et al., 1993). The order parameter for the $\phi$ and $\psi$ torsion angles for the majority of the residues in the structured region (residues 7−66) is >0.93, indicating that the backbone of the structures is well-defined (Figure 5C,D) with the exception of residues Cys-7 and Gln-8. The order parameter of Cys-7 for $\phi$ and of Gln-8 for $\psi$ is 0.8. Examination of the structures showed that the backbone of these residues adopts two distinct conformations: a major conformation (27 structures) and a minor conformation (3 structures). This implies that this part of the protein either

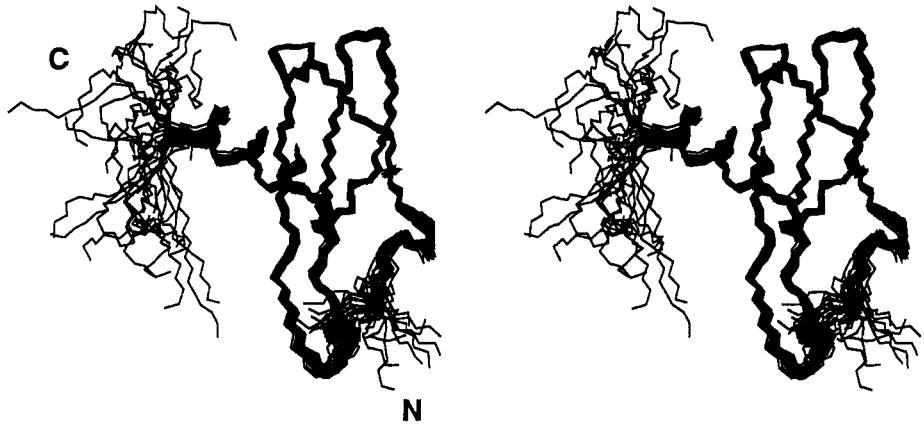


FIGURE 4: Stereoview showing the best fit superposition of the backbone (N, $C^{\alpha}$, C) atoms of the 30 simulated annealing structures. All residues (4−72) are shown though the superposition was carried out for residues 7−66.

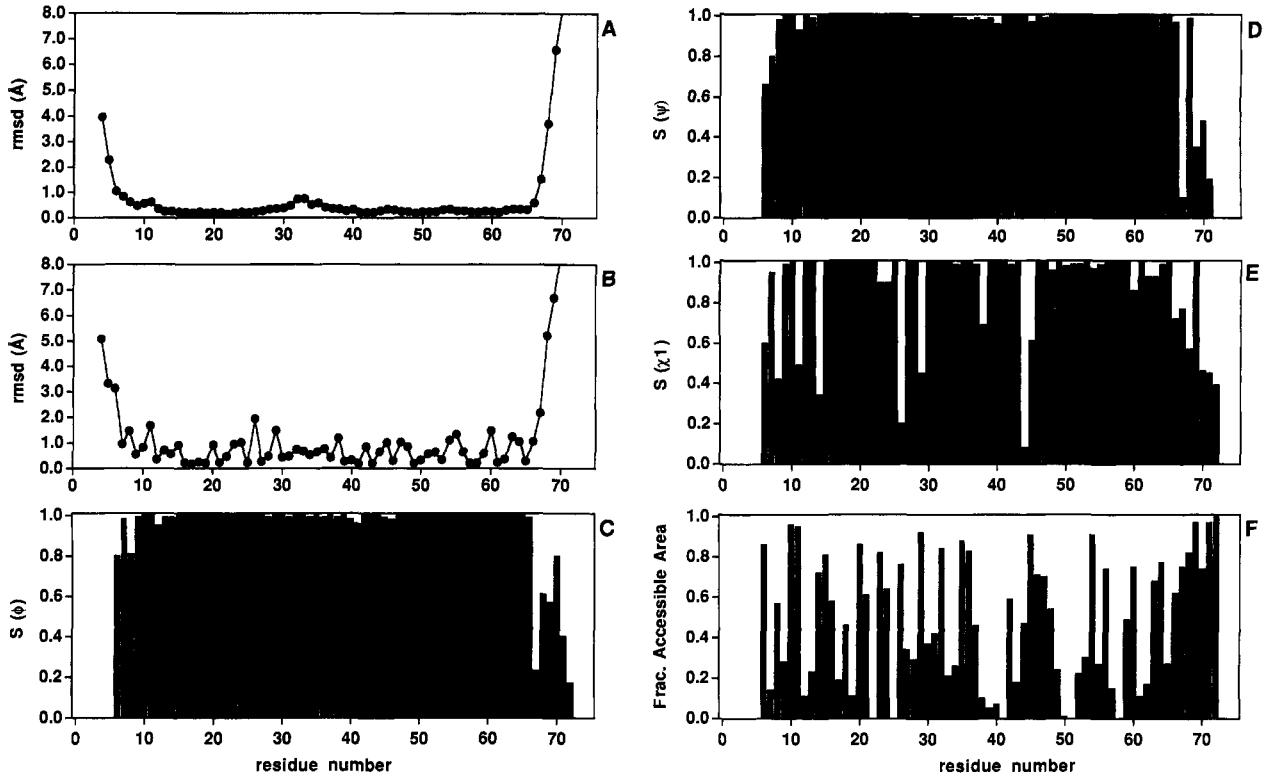


FIGURE 5: Atomic rms distribution of the 30 individual simulated annealing structures about the average structure best fitted for residues 7−66 for the backbone atoms (A) and all heavy atoms (B). Also shown are the angular order parameter ($S$) for $\phi$ (C), the angular order parameter ($S$) for $\psi$ (D), the angular order parameter ($S$) for $\chi_1$ (E), and fractional solvent-accessible area (F).

is relatively more mobile or is less defined due to chemical shift degeneracy and/or lack of NOEs. It is very likely that the conformational heterogeneity is due to the latter as the minor conformation adopts $\phi$ and $\psi$ angles which fall in the disallowed region of the Ramachandran plot. Figure 6 shows the Ramachandran plot of the backbone torsion angles of the well-defined region (residues 7−66) of the 30 individual SA structures and the energy-minimized average structure. It is seen that all of the torsion angles (except two of Gln-8) in all 30 structures fall in the "allowed" region.

The majority of the side chains, especially of the residues in the structured regions of the protein, are well-defined and are shown in Figure 7. Figure 5E shows that the side chains of most of the residues have order parameters ($S$) close to 1. Lower $S$ values are observed for charged residues such as Arg (26, 60), Lys (11, 15, 23, 54), Asp (45), and Glu (24, 29, 63). These charged residues tend to be located on the surface of the protein as indicated by the calculated fractional accessible surface area (ASA) (Figure 5F) (Lee & Richards, 1974). Side chains of residues Lys-23, Asp-24, Arg-26, and Glu-29 are part of the first $\beta$ strand which constitutes the dimer interface in the native IL-8. Glu-38 also exhibits a lower $S$ value, suggesting that it is disordered but it is significantly buried in all of the structures (ASA < 0.2).

*Solution Structure of Monomeric IL-8 (L25NMe).* The structure of the L25NMe monomer consists of a series of turns and loops at the N-terminus followed by three $\beta$ strands and a C-terminal $\alpha$ helix (Figure 8). The first $\beta$ strand (residues 22−29) is connected by a type III turn to the second $\beta$ strand (residues 38−42) which is connected by a type I turn to the third $\beta$ strand (47−52). The third strand leads into the helix (56−66) via a type III turn. There are four cysteines, all of which are involved in disulfide bond formation: Cys-7 forms a disulfide with Cys-34, which is

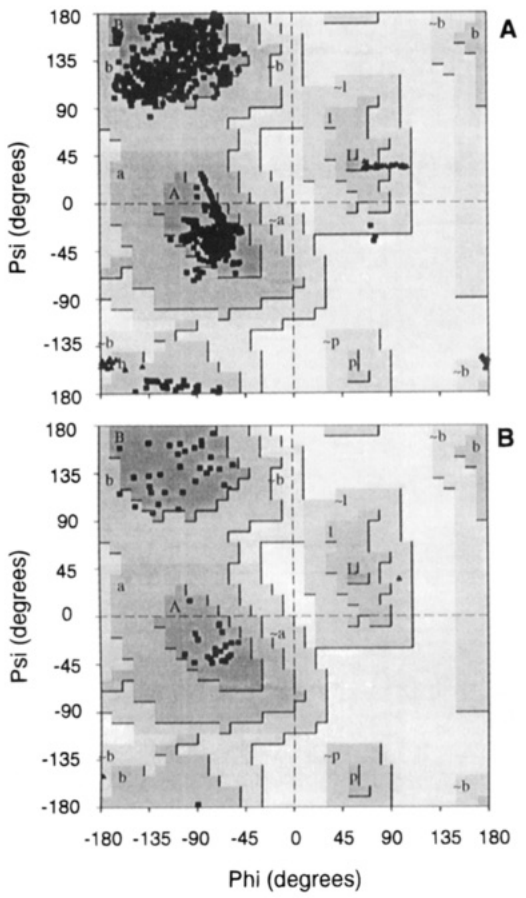


FIGURE 6: Ramachandran plot of the $\phi$, $\psi$ angles for residues 7−66 of (A) 30 simulated annealing structures and (B) the minimized average structure of the L25NMe IL-8 monomer. Glycines are shown as triangles. The regions denoted as A, B, and L are the most favored; a, b, l, and p are the additional allowed; and ~a, ~b, ~l, and ~p are the generously allowed. The plot is generated using the program PROCHECK (Laskowski et al., 1993).

part of the turn linking the first and second $\beta$ strands and Cys-9 forms a disulfide bond with Cys-50 of the third $\beta$ strand. Residues 4−6 and 67−72 are unstructured. The secondary and tertiary structural elements of the monomeric L25NMe analog are largely similar to that of the NMR and X-ray structures of the dimeric IL-8 (Figure 9). Superimposition of the backbone atoms of the monomeric structure on the dimeric NMR and X-ray structures for residues 7−66 gives an rms difference of 1.2 Å for the X-ray structure and 1.5 Å for the NMR structure. Comparison of the dihedral angles ($\phi$, $\psi$) for residues 7−66 showed no significant differences between the monomeric and dimeric structures. However, the differences are more pronounced between the monomeric and the dimeric NMR structure than the dimeric X-ray structure. Similarly, the side-chain $\chi_1$ values were largely the same between the structures and, if different, were confined to surface residues that were mostly undefined in the individual SA structures. Also, the fractional ASAs of the monomeric and the dimeric structures were similar except for the residues at the dimer interface. In the monomer, the residues of the first $\beta$ strand, which normally constitute the dimer interface, retain their $\beta$ structure as evident by their strong $i$, $i$+1 NOEs and the long-range NOEs with residues of the second $\beta$ strand. One of the more significant differences between the monomer and the dimer structures is observed at the C-terminal helix. In the dimer, the helix extends all the way up to the second last residue (Asn-71), whereas in the monomer, the helix as evident by the strong $NH_iNH_{i+1}$ and $i$, $i$+3 NOEs extends only up to Leu-66, with the remaining residues being disordered. For residues 67−72, only sequential NOEs were observed and no long- or medium-range NOEs were evident. These observations are also consistent with the $C^{\alpha}H$ shifts, which suggest a random coil structure (Wishart et al., 1991).

Residue to residue backbone rms difference between the monomeric and dimeric structures is shown in Figure 10. It is seen that the monomer is more similar to the dimeric X-ray structure (Baldwin et al., 1991) than to the NMR structure (Clore et al., 1990). The major differences are in turn residues 31−35 and the N-terminal residues 4−6, which are disulfide-linked to one another via Cys-7 and Cys-34. The rms difference between the monomeric and the dimeric NMR structures without the turn residues (31−35) is 1.3 Å, a value similar to that seen between the monomer and the X-ray structure. The rms difference between the two dimeric structures for residues 31−35 is 2.7 Å and was attributed to the differential interaction of the His-33 and also of the Glu-29 side-chain atoms in the two structures (Clore & Gronenborn, 1991). In the X-ray structure, His-33 $N^{\epsilon 2}$ donates a hydrogen bond to the backbone carbonyl of Glu-29 whereas in the NMR structure it accepts a hydrogen bond from the Gln-8 NH. Also, in the X-ray structure, there is an electrostatic interaction between Glu-4 and Lys-23′ across the dimer interface, whereas in the NMR structure, there is an electrostatic interaction between Glu-29 and Lys-23′ across the dimer interface. In the monomer, the His-33 side chain adopts an orientation similar to that in the X-ray structure and is in hydrogen-bonding distance from the carbonyl of Glu-29. The chemical shifts of the residues in the 31−35 turn and the N-terminal residues 7−9, which include the C-X-C motif, are similar to that seen in the dimeric NMR structure. This includes Gln-8 NH (~11.8 ppm) and Cys-34 NH (~6.8 ppm), which show large downfield and upfield chemical shifts, respectively. The downfield shift of the Gln-8 NH was attributed to the hydrogen bonding to the His-33 $N^{\epsilon 2}$ in the dimer structure (Clore et al., 1990). However, this amide proton is downfield shifted in an analog lacking His-33 (H33A), suggesting other structural features are responsible (Rajarathnam et al., 1994b). A similarly downfield-shifted Gln-8 and an upfield-shifted Cys-34 are also observed in MGSA/Gro-α (Kim et al., 1994), and as in the case of IL-8, mutation of the residue corresponding to His-33 had no effect on the Gln-8 chemical shift (Kim et al., 1994). NMR studies of truncation and substitution analogs of the N-terminus and the 31−35 turn had shown that the turn region is mobile and the disulfide bond to the N-terminus modulates its mobility. We had suggested that the structural differences between the NMR and the X-ray structures are of little functional relevance and are a consequence of the methods used (Rajarathnam et al., 1994a). Hence, the observation that the monomer structure for the 31−35 turn is similar to that in the X-ray structure is consistent with our previous observations and suggests that this part of the protein can undergo significant segmental motion. Comparison of the structures of IL-8 and MGSA also showed significant differences in the turn region (Kim et al., 1994; Fairbrother et al., 1994). Dynamic studies using $^{13}C$ and $^{15}N$ nuclei in the monomer should provide a more quantitative assessment of the differences, if any, for this part of the protein. Residues 4−6 are disordered in the IL-8

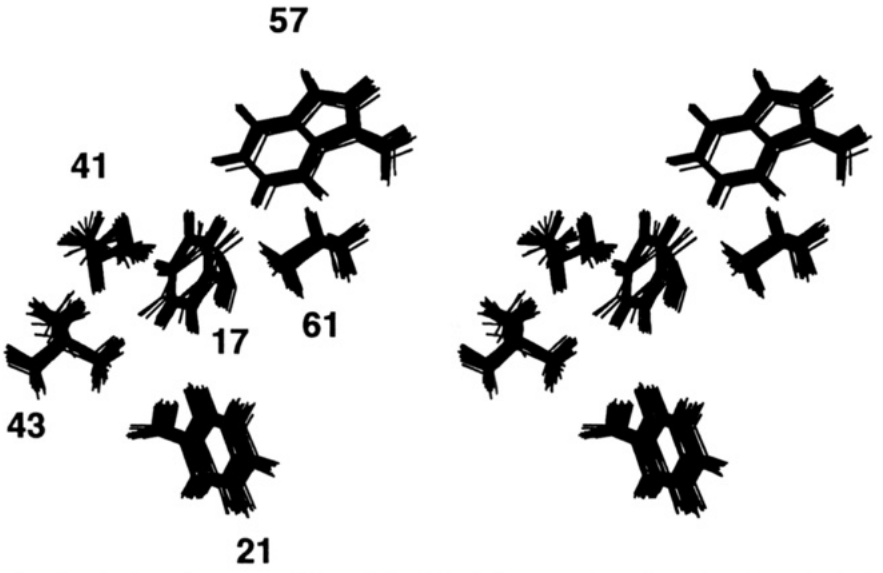


FIGURE 7: Stereoview showing the best fit superposition of the side-chain atoms for selected residues in the 30 SA structures of the L25NMe IL-8 monomer.

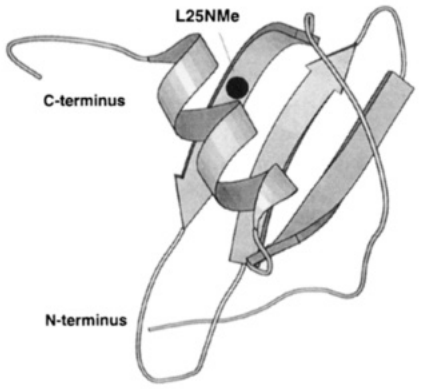


FIGURE 8: Schematic diagram showing the restrained minimized average structure of the L25NMe IL-8 monomer. The figure was created using the program MOLSCRIPT (Kraulis, 1991).

monomer, as they are in the NMR dimeric structure. However, the observation that the average orientation of these residues in the monomer is similar to that seen in the dimeric X-ray structure and different from that in the NMR dimeric structure is most likely due to the differential orientation of the 31−35 turn.

A number of dimeric proteins lose their tertiary structure upon dissociation (Bowie & Sauer, 1989; Grant et al., 1992; Neet & Timm, 1994). In the case of IL-8, its structure is largely retained, although there is some "loosening" of the structure which can be attributed to the loss of quaternary interactions. In addition to the C-terminal residues 67−72 becoming disordered, the hydrogen-exchange rate of the labile amide protons are considerably faster (Rajarathnam et al., 1994b). The exchange rate of the amide protons is a good indication of the stability of the secondary and tertiary structures such as the α-helix and β-sheet. Though the secondary and tertiary structural characteristics are retained in the monomer, faster exchange kinetics suggest greater mobility and/or flexibility which may have relevance for receptor binding and functional activation. This is suggested by an experiment in which an IL-8 analog was covalently linked across the dimer interface by two disulfide bonds (K23C and G31C). This analog was completely inactive (I. Clark-Lewis, B. Dewald, and M. Baggiolini, unpublished results), and this loss of activity could be directly attributed to the loss of flexibility. The observation that the monomer structure is largely similar to the IL-8 dimer structures (Baldwin et al., 1991; Clore et al., 1990) and to the tertiary structure of the other C-X-C family of proteins such as MGSA/Gro-α (Kim et al., 1994; Fairbrother et al., 1994), NAP-2 (Malkowski et al., 1995), and PF-4 (Zhang et al., 1994) and to those of the C-C family of proteins such as MIP-1β (Lodi et al., 1994) and RANTES (Skelton et al., 1995) suggests that the global fold and stability are dictated by the two disulfide bonds (Cys-7 and Cys-34; Cys-9 and Cys-50). These disulfides have been shown to be essential, and pairwise substitution of corresponding cysteines results in loss of activity and also loss of tertiary structure (Clark-Lewis et al., 1991).

*Structure and Function.* All available data to date indicate that the active species of IL-8 is a monomer. The measured $K_d$ value of ~20 μM suggests that, at normal functional concentrations (~0.1−10 nM), the dominant species is the monomer (Burrows et al., 1994; Paolini et al., 1994). Sedimentation equilibrium studies indicate that MGSA/Gro-α and NAP-2, which belong to the IL-8 family, have similar or lower $K_d$ values (~20−100 μM) (Rajarathnam et al., unpublished results), reiterating that the active species for these proteins is the monomer.

Functional studies showed that the most crucial residues for activity are the N-terminal residues Glu-4, Leu-5, and Arg-6 ("ELR" motif). Mutation or deletion of these residues results in a large decrease in binding and function (Hébert et al., 1991; Clark-Lewis et al., 1991). In addition, residues 10−22 and 31−34 were also shown to be essential (Clark-Lewis et al., 1994). However, isolated peptides corresponding to these regions were completely inactive. This suggests that the core of the protein acts as a scaffold from which the flexible N-terminal residues (4−6) and the other residues are suspended in a way which facilitates receptor binding and neutrophil activation. Of the two receptors identified for neutrophils, one (IL-8R2) binds IL-8, NAP-2, and MGSA with equal affinity and the other (IL-8R1) binds IL-8 with high affinity and NAP-2 and MGSA with low affinity (Moser et al., 1991; Lee et al., 1992). In addition, a nonspecific receptor for Duffy antigen which binds both CXC and CC

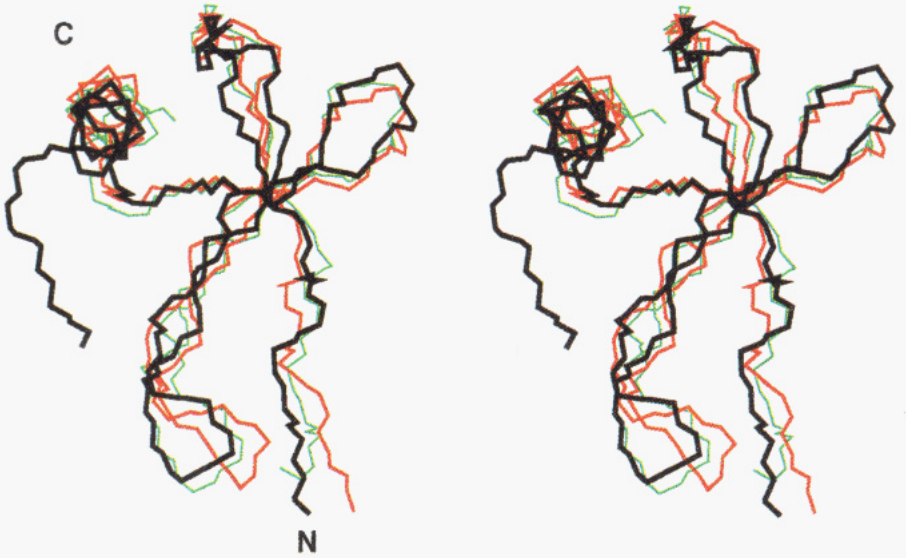


FIGURE 9: Stereoview showing the best fit superposition of the minimized average monomeric NMR (black) and the dimeric NMR (red) and X-ray (green) structures.

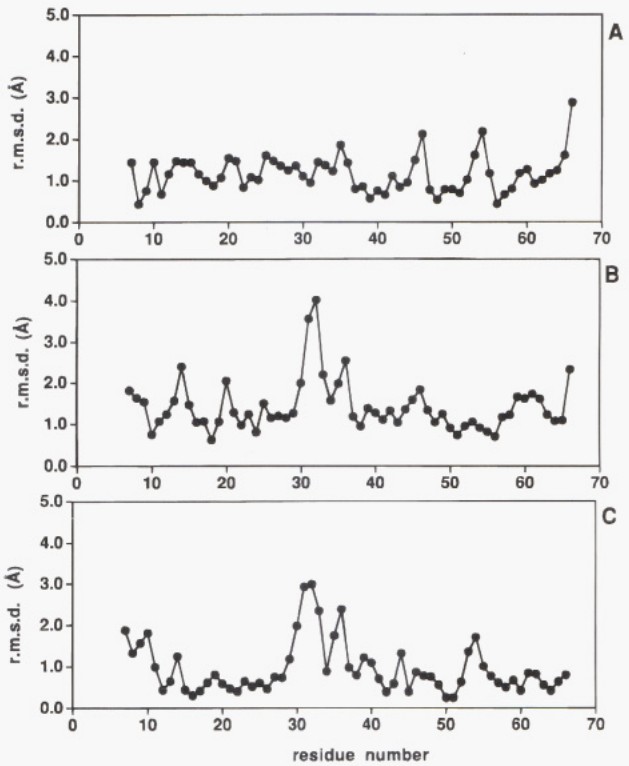


FIGURE 10: Best fit superposition using residues 7−66 for the backbone atoms between (A) the L25NMe monomer and X-ray dimer, (B) the L25NMe monomer and NMR dimer, and (C) the NMR dimer and X-ray dimer.

chemokines with fairly high affinity has been identified (Horuk et al., 1993). As the monomer is the functional unit, the knowledge of the structure of the monomer is critical in our understanding of IL-8 structure−function relationship.

The core of the monomer structure is essentially the same as the dimeric NMR and X-ray structures. Interestingly, the $\beta$ strand which forms the dimer interface in the dimeric structure retains its structure in the monomer. The introduction of the bulky methyl group, though disrupting the dimer formation, has minimal effect on the secondary and tertiary structure interactions within the monomer. The functionally critical "ELR" motif is disordered as observed in the dimeric NMR structure. The structure of the monomer for residues 10−22, which has been shown to be critical for function (Clark-Lewis et al., 1994), is largely the same as in the dimeric NMR and X-ray structures. Comparison of the MGSA and IL-8 structures has shown subtle but distinct differences in the regions considered critical for function, i.e., the "ELR" motif, the 31−35 turn, and the loops between residues 12 and 23 (Kim et al., 1994; Fairbrother et al., 1994). It has been proposed that the "ELR" motif constitutes the primary binding site on the receptor and the 12−23 region constitutes the secondary binding site and is responsible for receptor specificity (Clark-Lewis et al., 1995; Fairbrother et al., 1994). Glu-38 is unusual as it is buried in all of the 30 structures and in the average structure of the L25NMe monomer. Though the side chain is disordered, the carboxylate group is pointed in the direction of the N-terminal residues in all of the structures. A similar orientation for this residue is observed in both the NMR and the X-ray dimeric structures. This residue is conserved among all known C-X-C chemokines except PF-4 in which it is conservatively substituted with a Gln. This suggests that this residue may have a functional role in its ability to interact with the N-terminus, and future substitution studies should confirm whether this is the case.

The loss of structure for residues 67−72 in the monomer can be directly attributed to the disruption of the dimeric structure. In the dimer, the C-terminal helix runs across the dimer interface and is stabilized by interactions across the dimer interface. The structure of MGSA, which has been solved by NMR spectroscopy, has a tertiary and quaternary structure similar to that of IL-8 (Kim et al., 1994; Fairbrother et al., 1994). However, the dimer interface is weaker as inferred by the hydrogen-exchange and sedimentation equilibrium studies (Kim et al., 1994), which is also reflected in the last four residues of the C-terminal helix being unstructured. The observation that the C-terminal residues 67−72 are unstructured in the IL-8 monomer is of no relevance to neutrophil activation as the truncated IL-8 analog 4−66 has shown activity similar to that of the native protein (Clark-Lewis et al., 1991). However, the flexible C-terminus may have a role *in vivo* as it is the cell-surface-bound IL-8 which binds to the neutrophil receptors (Rot, 1992a). It has been proposed (Rot, 1992b), and there is experimental evidence

which suggests, that the C-terminal helix binds to heparin and heparin sulfate on the cell surface (Webb et al., 1993) and hence may have relevance in the dynamics of the IL-8 binding *in vivo*.

## ACKNOWLEDGMENT

We thank Key-Sun Kim and Stéphane Gagne for helpful discussions and advice; David Wishart, Frank Söennichsen, and Wolfram Gronwald for critical reading of the manuscript; Gerry McQuaid and Leigh Willard for technical support; and Philip Owen, Peter Borowski, and Luan Vo for the protein synthesis.

## SUPPORTING INFORMATION AVAILABLE

One table containing the $^1$H NMR chemical shifts of the monomeric L25NMe interleukin-8 (2 pages). Ordering information is given on any current masthead page.

## REFERENCES

Baggiolini, M., Dewald, B., & Moser, B. (1994) *Adv. Immunol. 55*, 97−179.

Baldwin, E. T., Weber, I. T., Charles, R., Xuan, J.-C., Appella, E., Yamada, M., Matsushima, K., Edwards, B. F. P., Clore, G. M., Gronenborn, A. M., & Wlodawer, A. (1991) *Proc. Natl. Acad. Sci. U.S.A. 88*, 502−506.

Basus, V. J. (1989) *Methods Enzymol. 177B*, 131−147.

Bothner-By, A. A., Stephens, R. L., Lee, J. T., Warren, C. D., & Teanloz, R. W. (1984) *J. Am. Chem. Soc. 106*, 811−813.

Bowie, J. U., & Sauer, R. T. (1989) *Biochemistry 28*, 7139−7143.

Brown, S. C., Weber, P. L., & Mueller, L. (1988) *J. Magn. Reson. 77*, 166−169.

Brünger, A. T. (1992) *X-PLOR. A System for X-ray Crystallography and NMR*, Yale University Press, New Haven, CT.

Burrows, S. D., Doyle, M. L., Murphy, K. P., Franklin, S. G., White, J. R., Brooks, I., McNulty, D. E., Scott, M. O., Knutson, J. R., Porter, D., Young, P. R., & Hensley, P. (1994) *Biochemistry 33*, 12741−12745.

Clark-Lewis, I., Schumacher, C., Baggiolini, M., & Moser, B. (1991) *J. Biol. Chem. 266*, 23128−23134.

Clark-Lewis, I., Dewald, B., Loetscher, M., Moser, B., & Baggiolini, M. (1994) *J. Biol. Chem. 269*, 16075−16081.

Clark-Lewis, I., Kim, K.-S., Rajarathnam, K., Gong, J.-H., Dewald, B., Moser, B., Baggiolini, M., & Sykes, B. D. (1995) *J. Leukocyte Biol. 57*, 703−711.

Clore, G. M., & Gronenborn, A. M. (1991) *J. Mol. Biol. 217*, 611−620.

Clore, G. M., Gronenborn, A. M., Nilges, M., & Ryan, C. A. (1987) *Biochemistry 26*, 8012−8023.

Clore, G. M., Appella, E., Yamada, M., Matsushima, K., & Gronenborn, A. M. (1990) *Biochemistry 29*, 1689−1696.

Davis, D. G., & Bax, A. (1985) *J. Am. Chem. Soc. 107*, 2821−2822.

Fairbrother, W. J., Reilly, D., Colby, T. J., Hesselgesser, J., & Horuk, R. (1994) *J. Mol. Biol. 242*, 252−270.

Gayle, R. B., Sleath, P. R., Srinivason, S., Birks, C. W., Weerawarna, K. S., Cerretti, D. P., Kozlosky, C. J., Nelson, N., Bos, T. V., & Beckmann, M. P. (1993) *J. Biol. Chem. 268*, 7283−7289.

Grant, S. K., Deckman, I. C., Culp, J. S., Minnich, M. D., Brooks, I. S., Hensley, P., Debouck, C., & Meek, T. D. (1992) *Biochemistry 31*, 9491−9501.

Hébert, C. A., Vitangcol, R. V., & Baker, J. B. (1991) *J. Biol. Chem. 266*, 18989−18994.

Heinz, D. W., Hyberts, S. G., Peng, J. W., Priestle, J. P., Wagner, G., & Grutter, M. G. (1992) *Biochemistry 31*, 8755−8766.

Holmes, W. E., Lee, J., Kuang, W.-J., Rice, G. C., & Wood, W. I. (1991) *Science 253*, 1278−1280.

Horuk, R., Chitnis, C. E., Darbonne, W. C., Colby, T. J., Rybicki, A., Hadley, T. J., & Miller, L. H. (1993) *Science 261*, 1182−1184.

Hyberts, S. G., Goldberg, M. S., Havel, T. F., & Wagner G. (1992) *Protein Sci. 1*, 736−751.

Jeener, J., Meier, B. H., Bachmann, P., & Ernst, R. R. (1979) *J. Chem. Phys. 71*, 4546−4553.

Kim, K.-S., Clark-Lewis, I., & Sykes, B. D. (1994) *J. Biol. Chem. 269*, 32909−32915.

Kim, Y., & Prestegard, J. H. (1989) *J. Magn. Reson. 84*, 9−13.

Kraulis, P. (1991) *J. Appl. Crystallogr. 24*, 946−950.

Laskowski, R. A., MacArthur, M. W., Moss, D. S., & Thornton, J. M. (1993) *J. Appl. Crystallogr. 26*, 283−291.

Lee, B., & Richards, F. M. (1971) *J. Mol. Biol. 55*, 379−400.

Lee, J., Horuk, R., Rice, G. C., Bennett, G. L., Camerato, T., & Wood, W. I. (1992) *J. Biol. Chem. 267*, 16283−16287.

Lodi, P. J., Garrett, D. S., Kuszswski, J., Tsang, M. L.-S., Weatherbee, J. A., Leonard, W. J., Gronenborn, A. M., & Clore, G. M. (1994) *Science 263*, 1762−1766.

Malkowski, M. G., Wu, J. Y., Lazar, J. B., Johnson, P. H., & Edwards, B. F. P. (1995) *J. Biol. Chem. 270*, 7077−7087.

Miller, M. D., & Krangel, M. S. (1992) *Crit. Rev. Immunol. 12*, 17−46.

Moser, B., Schumacher, C., von Tscharner, V., Clark-Lewis, I., & Baggiolini, M. (1991) *J. Biol. Chem. 266*, 10666−10671.

Mueller, L. (1987) *J. Magn. Reson. 72*, 191−196.

Neet, K. E., & Timm, D. E. (1994) *Protein Sci. 3*, 2167−2174.

Nicholas, J. S., Aspiras, F., Ogez, J., & Schall, T. J. (1995) *Biochemistry 34*, 5329−5342.

Nilges, M., Clore, G. M., & Gronenborn, A. M. (1988) *FEBS Lett. 229*, 317−324.

Pallaghy, P. K., Duggan, B. M., Pennington, M. W., & Norton, R. S. (1993) *J. Mol. Biol. 234*, 405−420.

Paolini, J. F., Willard, D., Consler, T., Luther, M., & Krangel, M. S. (1994) *J. Immunol. 153*, 2704−2717.

Pardi, A., Wagner, G., & Wüthrich, K. (1983) *Eur. J. Biochem. 137*, 445−454.

Powers, R., Garret, D. S., March, C. J., Frieden, E. A., Gronenborn, A. M., & Clore, G. M. (1993) *Biochemistry 32*, 6744−6762.

Rajarathnam, K., Clark-Lewis, I., & Sykes, B. D. (1994a) *Biochemistry 33*, 6623−6630.

Rajarathnam, K., Sykes, B. D., Kay, C. M., Dewald, B., Geiser, T., Baggiolini, M., & Clark-Lewis, I. (1994b) *Science 264*, 90−92.

Rance, M., Sørensen, O. W., Bodenhausen, G., Wagner, G., Ernst, R. R., & Wüthrich, K. (1983) *Biochem. Biophys. Res. Commun. 117*, 479−485.

Rot, A. (1992a) *Cytokine 4*, 346−352.

Rot, A. (1992b) *Immunol. Today 13*, 291−293.

States, D. J., Haberkorn, R. A., & Ruben, D. J. (1982) *J. Magn. Reson. 48*, 286−292.

Wagner, G., Braun, W., Havel, T. F., Schaumann, T., Gö, N., & Wüthrich, K. (1987) *J. Mol. Biol. 196*, 611−639.

Webb, L. M. C., Ehrengruber, M. U., Clark-Lewis, I., Baggiolini, M., & Rot, A. (1993) *Proc. Natl. Acad. Sci. U.S.A. 90*, 7158−7172.

Wishart, D. S., Sykes, B. D., & Richards, F. M. (1991) *J. Mol. Biol. 222*, 311−333.

Wishart, D. S., Willard, L., & Sykes, B. D. (1994) *VADAR, Version 1.2*, University of Alberta.

Wüthrich, K. (1986) *NMR of Proteins and Nucleic Acids*, John Wiley & Sons, New York.

Wüthrich, K., Billeter, M., & Braun, W. (1983) *J. Mol. Biol. 169*, 949−961.

Zhang, X., Chen, L., Bancroft, D. P., Lai, C. K., & Maione, T. E. (1994) *Biochemistry* 33, 8361−8366.

BI9512206